Anatomical Organization of the Visual Dorsal Ventricular Ridge in the Chick (*Gallus gallus*): Layers and Columns in the Avian Pallium

Patricio Ahumada-Galleguillos,[1,2] Máximo Fernández,[1] Gonzalo J. Marin,[1,3] Juan C. Letelier,[1] and Jorge Mpodozis[1]*

[1]Departamento de Biologia, Facultad de Ciencias, Universidad de Chile, Santiago, Chile
[2]Biomedical Neuroscience Institute, Anatomy and Developmental Biology Program, Institute of Biomedical Sciences, Facultad de Medicina, Universidad de Chile, Santiago, Chile
[3]Facultad de Medicina, Universidad Finis Terrae, Santiago, Chile

ABSTRACT

The dorsal ventricular ridge (DVR) is one of the main components of the sauropsid pallium. In birds, the DVR is formed by an inner region, the nidopallium, and a more dorsal region, the mesopallium. The nidopallium contains discrete areas that receive auditory, visual, and multisensory collothalamic projections. These nidopallial nuclei are known to sustain reciprocal, short-range projections with their overlying mesopallial areas. Recent findings on the anatomical organization of the auditory DVR have shown that these short-range projections have a columnar organization that closely resembles that of the mammalian neocortex. However, it is unclear whether this columnar organization generalizes to other areas within the DVR. Here we examine in detail the organization of the visual DVR, performing small, circumscribed deposits of neuronal tracers as well as intracellular fillings in brain slices. We show that the visual DVR is organized in three main laminae, the thalamorecipient nucleus entopallium; a dorsally adjacent nidopallial lamina, the intermediate nidopallium; and a contiguous portion of the ventral mesopallium, the mesopallium ventrale. As in the case of the auditory DVR, we found a highly topographically organized system of reciprocal interconnections among these layers, which was formed by dorsoventrally oriented, discrete columnar bundles of axons. We conclude that the columnar organization previously demonstrated in the auditory DVR is not a unique feature but a general characteristic of the avian sensory pallium. We discuss these results in the context of a comparison between sauropsid and mammalian pallial organization. J. Comp. Neurol. 523:2618–2636, 2015.

© 2015 Wiley Periodicals, Inc.

The pallial telencephalon is considered the most variable and diverse region in the brains of amniotes (Striedter, 1997; Butler and Hodos, 2005; Murakami et al., 2005; Sol et al., 2010). In mammals, the cortical pallial territories have a multilayered organization in which cells of the different layers are functionally connected by radially oriented processes, which form restricted local circuits between layers. Because of this intrinsic connectivity, neurons included in a columnar section radially oriented across the layers tend to have common physiological properties and are regarded as forming operational modules (Gilbert and Wiesel, 1989; Mountcastle, 1997; Da Costa and Martin, 2010). In contrast, the pallial region of nonmammalian amniotes seems very different from the cortex; it does not

appear to have a laminar structure, and, until recently (see below), no functional modules or recurrent local circuits have been described for it (Jarvis et al., 2005).

One of the main components of the sauropsid pallium corresponds to the dorsal ventricular ridge (DVR), whose pallial nature has been confirmed according to multiple criteria, including overall connectivity, embryogenesis, expression of molecular markers, and topology

(Reiner et al., 2004; Dugas-Ford et al., 2012; Jarvis et al., 2013). In birds, the DVR is formed by an inner region known as the nidopallium and a more dorsal area known as the mesopallium. The former contains discrete areas that receive auditory (derived from the thalamic nucleus ovoidalis), visual (derived from the thalamic nucleus nucleus rotundus), and multisensory (derived from the thalamic nucleus nucleus dorsolateralis posterioris) collothalamic projections (Korzeniewska and Gunturkun, 1990; Hodos and Butler, 2005). The presence of these collorecipient regions within the DVR has been one of the main criteria leading to the proposed homological correspondence between the DVR and the mammalian extrastriate cortex (Karten, 1969; Butler et al., 2011).

The anatomical organization of the auditory DVR, the hodological equivalent of the mammalian auditory cortex, has been recently investigated in detail in chicks by Wang et al. (2010). This region is composed of two major cytoarchitectonic zones, the nidopallial field L, receiving auditory afferents from the thalamic nucleus ovoidalis (homologous to the ventral division of the mammalian medial geniculate nucleus), and a dorsally adjacent mesopallial region, the caudal mesopallium (CM). Wang et al. showed that the field L and the CM constitute a system of layered cell groups (field L2a, L1 internus, L1 externus, L3) extensively interconnected by discrete columnar bundles of axons oriented perpendicular to the laminae. These axonal bundles form reciprocal, topographically organized, homotopical projections among cells located in the main thalamorecipient layer (field L2a) and cells located in the dorsally adjacent L1and CM. Based on these results, Wang et al. (2010) compared the organization of the field L/CM complex with that of the columns of the mammalian auditory cortex, proposing the existence of a correspondence at laminar, cellular, and intrinsic circuitry levels.

Whether this type of columnar organization is a particular feature of the field L or a general characteristic of the sensory DVR remains at present an open question. In this regard, the current literature contains several hints suggesting that the visual DVR may also be organized as a system of interconnected laminae. The visual DVR is composed of three main cytoarchitectonic zones, an internal one, the entopallium (E), that is the main recipient of visually driven projections from the nucleus rotundus (homologous to the mammalian caudal pulvinar nucleus); an overlaying nidopallial region, which we will call intermediate nidopallium (NI), referred in the literature as "entopallial belt" or "perientopallium" (see Discussion); and a dorsally adjacent mesopallial region, the nucleus mesopallialis ventrolaterale (MVL; Benowitz and Karten, 1976; Husband

and Shimizu, 1999; Laverghetta and Shimizu, 2003; Fredes et al., 2010). Several studies have shown the existence of short-range projections connecting the E to the NI and the NI to farther rostral and caudal zones of the lateral pallium, forming a sequential arrangement that has been considered the "classic signature" of the DVR (Husband and Shimizu, 1999; Güntürkün and Kröner, 1999; Alpár and Tömböl, 2000). However, more recent works from Krützfeldt and Wild (2004, 2005) with the zebra finch and the pigeon indicate that the visual DVR has a much more complex organization than previously appreciated. In addition to confirming previous findings, these authors show that the rotundal endings innervate both the E and also, albeit more sparsely, the NI. Additionally they show that, besides targeting the NI, efferents from the E reach the underlying striatum and also the MVL. In turn, and most interestingly, cells of the MVL located close to the entopallial terminal field were shown to project back to the E, indicating the existence of reciprocal projections between the E and the MVL. At present, however, the detailed organization of this system of projections remains to be established.

Here we examine in detail the organization of the visual DVR in chicks (*Gallus gallus*), placing small, circumscribed injections of neuronal tracers as well as intracellular fillings in brain slices. We show that the visual DVR is composed of three differentiated, highly interconnected layers, internal (thalamorecipient, E), intermediate (efferent, NI), and external (associative, MV). As in the case of the auditory DVR, interconnections among these layers were formed by dorsoventrally oriented, discrete columnar bundles of axons that follow a precise topographic arrangement. We discuss these results in the context of a comparison of the pallial organization between sauropsids and mammals.

MATERIALS AND METHODS
Animals

In total 65 chicks (*Gallus gallus)* between 1 and 7 days posthatching were used. All the experimental procedures were approved by the Science Faculty's Ethics Committee, Universidad de Chile, and conformed to the guidelines of the National Institutes of Health (NIH) on the use of experimental animals in research.

Deposits of biocytin in vital slices

Forty chicks (P1–P5) were deeply anesthetized with a mixture (3:1) of 1% ketamine and 2% xylazine and then decapitated. The brains were quickly removed from the skull and submerged for 10 minutes in a cooled (4°C) chamber filled with sucrose-substituted Krebs solution
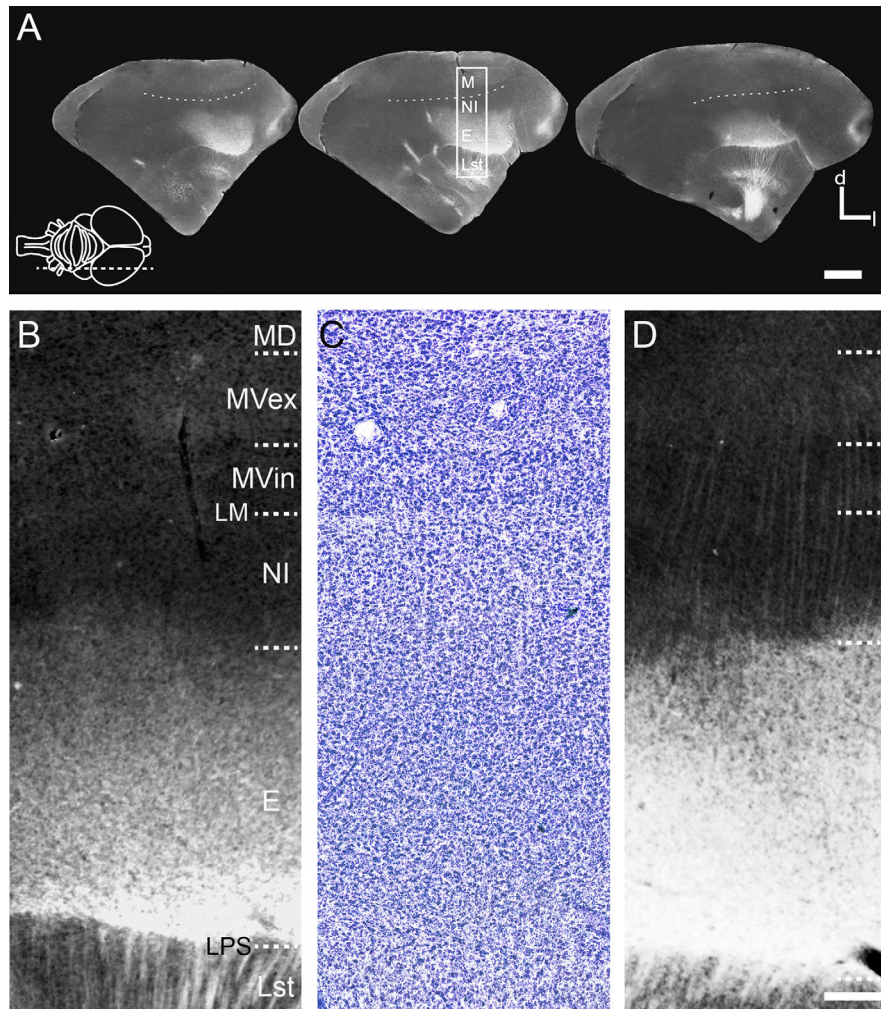
Figure 1. Characterization of the visual DVR. **A:** Sagittal series of unstained sections (50 μm) through the telencephalon of a hatching chick (2 days old). Both the entopallium (E) and the lateral striatum (LSt) are readily distinguishable. The lamina mesopallialis (LM, dashed line) can be approximated. Note in the lateralmost section (right) a bundle of rotundal axons coursing across the LSt toward the E. **B:** Detail of the boxed area in A. A faint, dusty-like opacity above the LM delimits the external lamina of the ventral mesopallium (MVex). **C:** Same section as in B stained with Nissl. Note the cytoarchitectonic differences among the different layers. Dashed lines in B indicated the apparent boundaries between layers. **D:** An equivalent wet, unstained section taken from a 10-day-old chick. Note the axonal processes running between the E and the MVex. The LM is also appreciable. NI, nidopallium intermedium; MVin, mesopallium ventrale, internal layer; MD, mesopallium dorsale; LPS, lamina palliosubpallialis. In this and subsequent figures, "d" bar indicates dorsal orientation and "l" bar indicates lateral orientation. The schema included in A indicates approximately the sagittal plane of section used in this study. Abbreviations apply to subsequent figures. Scale bar = 1 mm in A; 200 μm in D (applies to B-D).

(240 mM sucrose, 3 mM KCl, 3 mM MgCl$_2$, 23 mM NaHCO$_3$, 1.2 mM NaH$_2$PO$_4$, 11 mM D-glucose) continuously bubbled with carbogen (95% O$_2$, 5% CO$_2$). Brains were then manually blocked and sectioned at 500-1,000 μm on a vibratome (Leica VT 1200) in either the coronal or the sagittal plane. Brain slices were collected and submerged in a chamber containing artificial cerebrospinal fluid (ACSF; 119 mM NaCl, 2.5 mM KCl, 1.3 mM Mg$_2$SO$_4$, 1.0 mM NaH$_2$PO$_4$, 26.2 mM NaHCO$_3$, 11 mM D-glucose, 2.5 mM CaCl$_2$) at room temperature and continuously bubbled with carbogen. Sections were then transferred to a chamber filled with ACSF located on the stage of a dissecting microscope, and minute deposits of biocytin crystals (Sigma-Aldrich, St. Louis, MO; B4261) were manually placed under visual guidance in selected visual DVR locations, using a fine (100-μm tip diameter) tungsten needle. Different targets in the visual DVR were readily identified by the differential opacity that they exhibit in wet slices (Fig. 1). After the injections, the slices were maintained for approximately 5 hours in a chamber with ACSF solution and then fixed by immersion in 4% paraformaldehyde in 0.1 M phosphate buffer (pH 7.2). After 24 hours in the fixative solution, slices were transferred to a

cryoprotective 30% sucrose solution until they sank. Slices were then resectioned into 50–70-μm-thick sections with a freezing sliding microtome (Leitz 1400). The resulting sections were incubated in avidin-biotin-peroxidase complex solution (ABC Elite Kit; Vector Laboratories, Burlingame, CA) diluted 1:200 in PBS with 0.3% Triton X-100 for 1 hour at room temperature, then incubated for 5–7 minutes in 0.025% 3-3 diaminobenzidine (DAB; Sigma) with 0.01% hydrogen peroxide in PB, mounted on gelatin-coated slides, and stained with 0.05% osmium tetroxide for 30 seconds. Then, sections were dehydrated, cleared, and coverslipped with Permount (Fisher Scientific, Pittsburgh, PA). Selected sections were counterstained with Nissl (Merck cresyl violet acetate), to visualize the general divisions of the pallium and to corroborate the location of injection sites and terminal regions.

Deposits of DiI in fixed slices

Ten chicks were deeply anesthetized with the ketamine/xylazine mixture and perfused transcardially with 100 ml of 0.9% saline, followed by 100 ml of an ice-cold solution of 4% paraformaldehyde in 0.1 M phosphate buffer (pH 7.2). After the perfusion, the brains were excised and postfixed for 2–3 hours in the paraformaldehyde solution. Then, the brains were mounted on the stage of a vibratome (Campden Instruments 752M) and sliced at 500–1,500 μm in either the coronal or the sagittal plane. Slices containing the structures of interest were transferred to a dish located on the stage of a dissecting microscope. Deposits of crystals of DiI (Molecular Probes, Eugene, OR; D 282) onto the selected targets were achieved manually under visual guidance, with the aid of a fine needle. Injected slices were then incubated at 37°C for 2 weeks. After the incubation period, the slices were resectioned into 100-μm-thick sections with a vibratome (Leica VT 1200) and collected on gelatinized slides.

In vitro intracellular filling

These experiments followed the procedures described by Wang et al. (2006). Briefly, 15 animals (1–6 days posthatching) were deeply anesthetized with the ketamine/xylazine mixture and then quickly decapitated. The brains were removed and immediately transferred to a chamber containing cooled (4°C) sucrose-substituted Krebs solution. Middle and posterior brains were dissected, and the telencephalic hemispheres were manually split through the midline. From each hemisphere, sagittal 500-μm-thick slices were prepared and maintained as described above. Selected slices containing the visual DVR were then transferred to a chamber placed on the stage of an inverted microscope (Olympus BX51WI) and continuously perfused with carbogenated ACSF solution. Under these conditions, the structures of interest were clearly recognizable by the opacity differences. To fill neurons, we used sharp electrodes (60–90 MΩ) made of borosilicated capillary tubing (FHC; 1.5 mm × 0.75 mm) pulled in a vertical puller (Kopf model 720). The electrodes were backfilled with 5% biocytin-HCl (Sigma-Aldrich) in KAc 0.5 M, coupled to the head stage of an intracellular DC amplifier (Cygnus Technologies IR 183A), mounted on a three-axis hydraulic manipulator attached to the stage of the microscope, and manually approximated to the tissue surface. Target cells were visualized under infrared/DIC microscopy, and only healthy cells, recognizable by their irregular somatic profiles, were selected. Cell penetration, indicated by a sudden voltage drop, was achieved with a capacitive pulse. The tracer solution was iontophoretically injected into the neuron with 1–3 nA of positive current during 2–4 minutes. Slices containing filled cells were fixed overnight in 4% PFA in PBS 0.01 M and transferred to the cryoprotective sucrose solution until they sunk. Then, the slices were resectioned into 60-μm-thick sections with a freezing microtome (Leitz 1400). To reveal the filled neurons, the sections were treated with the ABC/DAB/osmium intensification protocol described above.

Data acquisition and analysis

Histological material was analysed, drawn, and photographed with a conventional epifluorescence microscope (Olympus BX61) equipped with a camera lucida attachment and coupled to a highly sensitive digital camera (Spot RT 100; Diagnostic Instruments, Sterling Heights, MI). Confocal images of selected sections were obtained with a microscope (Zeiss Axiovert 200) equipped with a spinning-disk confocal unit (PerkinElmer Ultraview; ×25 lens, 0.8 numerical aperture). Image contrast adjustments, annotations, and photomontage were performed in Adobe Photoshop. Final figures were prepared in Adobe Illustrator.

RESULTS

Characterization of the visual DVR

As stated in the introductory paragraphs, the visual DVR has been characterized mainly in adult pigeons and zebra finches and comprises three main dorsoventrally apposed regions: An internal nidopallial one, the entopallium (E), in receipt of dense afferents from the nucleus rotundus; an overlying nidopallial "girdle," which we call the nidopallium intermedium (NI) after Karten and Hodos (1967); and the portion of the ventral division of the mesopallium located above the NI,
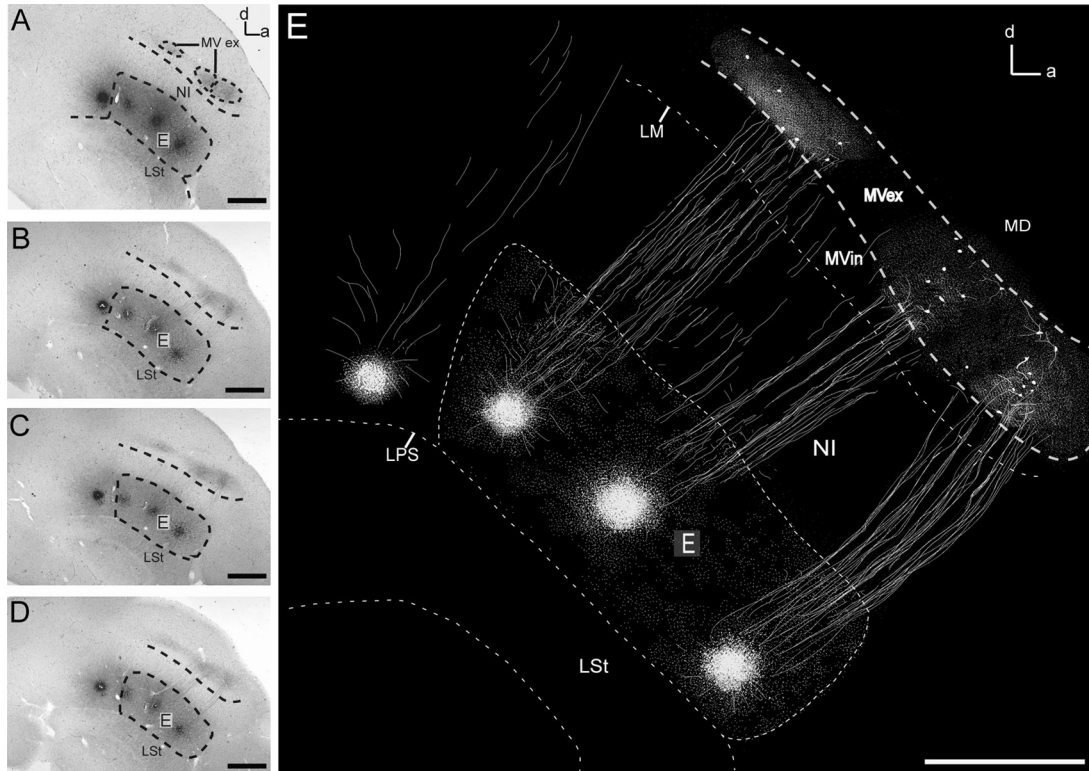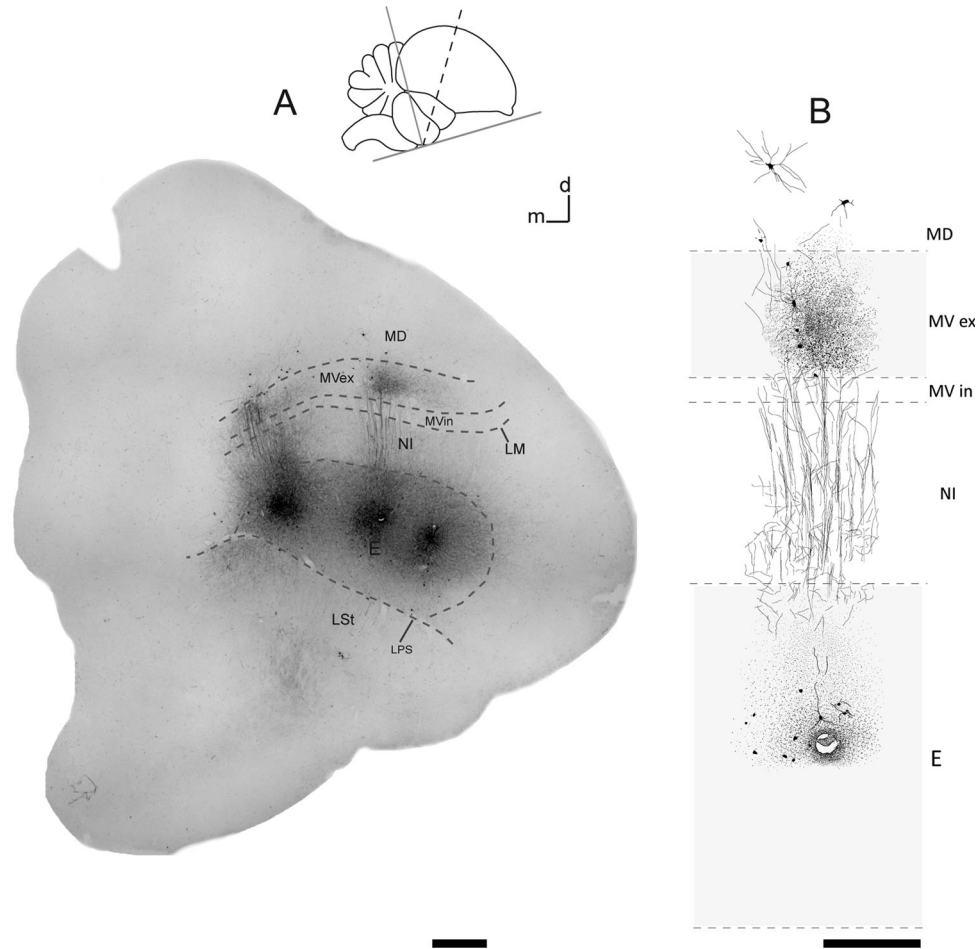
Figure 2. Multiple deposits of biocytin into the E in a sagittal vital slice (500 μm) of the visual DVR. **A-D:** Lateromedial series of histochemically reacted sections (50 μm) taken from the experimental slice. The dashed line ventral to the E indicates the lamina palliosubpallialis. The dashed line dorsal to the NI indicates the lamina mesopallialis. Limits of the E are also indicated by dashes. Note the axonal bundles running between each deposit site in the E and the MVex. At the MVex, discrete regions containing labeled terminals are readily appreciated (dash-bounded areas in A). **E:** Camera lucida reconstruction (Z projection) of the A-D series of sections. Contrast was reversed for better visualization. Boundaries between the different regions are indicated by dashed lines. Solid white represents crystal deposits. Solid lines represent axonal processes. Fine dots represent axonal terminals at the MVex and nonspecific labeling at the E. Note at the MVex the discrete patches of retrogradely labeled cells that appear to be immersed within the fields of labeled terminals. The posterior-most deposit, located outside the E, also originates a "column" of dorsally oriented labeled processes. In this and subsequent figures, "a" bar indicates anterior orientation. Scale bars = 1 mm.

designated by Reiner et al. (2004) as the mesopallium ventrale (MV). To define the visual DVR better in perinatal chicks, we examined sagittal series of wet unstained tissue as well as the corresponding series stained with Nissl (Fig. 1).

In wet tissue, the E was readily distinguishable as a zone of high opacity, consequent to the refractivity of the dense plexus of myelinated axons formed by the rotundal afferents (Krützfedt and Wild, 2005; Fredes et al., 2010). The lamina palliosubpallialis (LPS), marking the boundary between the E and the underlying lateral striatum (LSt), appeared clearly defined as well. The lamina mesopallialis (LM), delimiting the nidopallial/meso-pallial border, was barely evident in hatchling chicks but became conspicuous at 5 days posthatching (Fig. 1D). The NI was then easily identifiable as the region delimited by the LM and the external most entopallial border. At this stage, bundles of myelinated axons can be clearly

seen running across the NI, following a straight course between the E and the MV (Fig. 1D).

In Nissl stained material, the visual DVR features a complex, multilayered cytoarchitecture (Fig. 1C). The E appears as a uniform field of densely packed, small somata, with no evident subdivisions or stratifications. A subtle internal/external stratification, such as that described for other species at adult stages (Karten and Hodos, 1970; Krützfeldt and Wild, 2005; see Discussion), appeared in our material in some instances, but we were unable to find it consistently. The boundary between the E and the NI was clearly recognizable because the NI contained larger and less densely packed neurons clustered in dorsoventrally oriented rows, which are presumably organized along and between the columnar bundles of axons that run across the NI. The NI may contain further subdivisions because at central sagittal levels a thin and dense layer of cells,
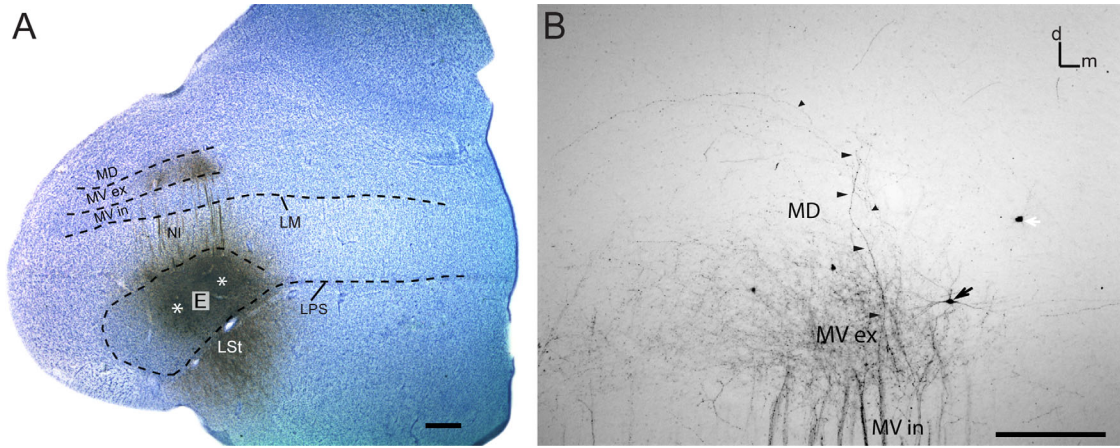
Figure 3. Multiple deposits of biocytin into the E in a transverse vital slice (500 μm) of the visual DVR. **A:** Histochemically reacted section (50 μm) taken from the experimental slice. Boundaries of the E appear clearly distinguishable. Note that the bundles of axons originating from the medial and central deposit ended in discrete terminal zones at the MVex. Some retrogradely labeled cell bodies around the terminal zones are also evident. **B:** Camera lucida reconstruction of the central "column" shown in A. Solid black represents crystal deposits. Solid lines represent axonal processes. Fine dots represent axonal terminals at the MVex and nonspecific labeling at the E. Note that retrogradely labeled cells are localized within and around the terminal zone. In this and subsequent figures, "m" bar indicates medial orientation. The schema in A indicates approximately the transverse plane of section used in this study. Scale bars = 200 μm.

located immediately above the entopallial boundary, is hinted at by the cytoarchitecture (not shown). The LM was readily distinguishable, and above it the MV appears stratified in two main layers, an internal one (MVint) and an external, cell-dense layer (MVex). The MVex is also hinted at in wet tissue, as a dusty-appearing, faint opacity band situated above the axonal bundles running between the E and the MV (Fig. 1B). Subsequent observations showed that the MVex, but not the MVint, is the main target of the entopallial projections (see below). Thus, MVex seems to correspond to the MVL described by Krützfeldt and Wild (2004) for the zebra finch. Above the MVex, the dorsal division of the mesopallium, designated as the mesopallium dorsale (MD) by Reiner et al. (2004), can be clearly distinguished because somata in the

MD appear larger and more sparsely distributed that those in the MV.

Local circuits in the visual DVR

We sought to unravel the connectivity between the main components of the visual DVR implementing three different "in vitro" experimental approaches: First, we prepared brain slices to perform minute, well-defined deposits of biocytin crystals (transverse 15 instances, sagittal 15 instances) in different components of the visual DVR. This approach was complemented by manual deposits of small lipophilic crystals (DiI; transverse 20 instances, sagittal 10 instances) on fixed slices. In addition, we attempted to perform intracellular fillings of the principal cellular morphotypes that compose the visual DVR.
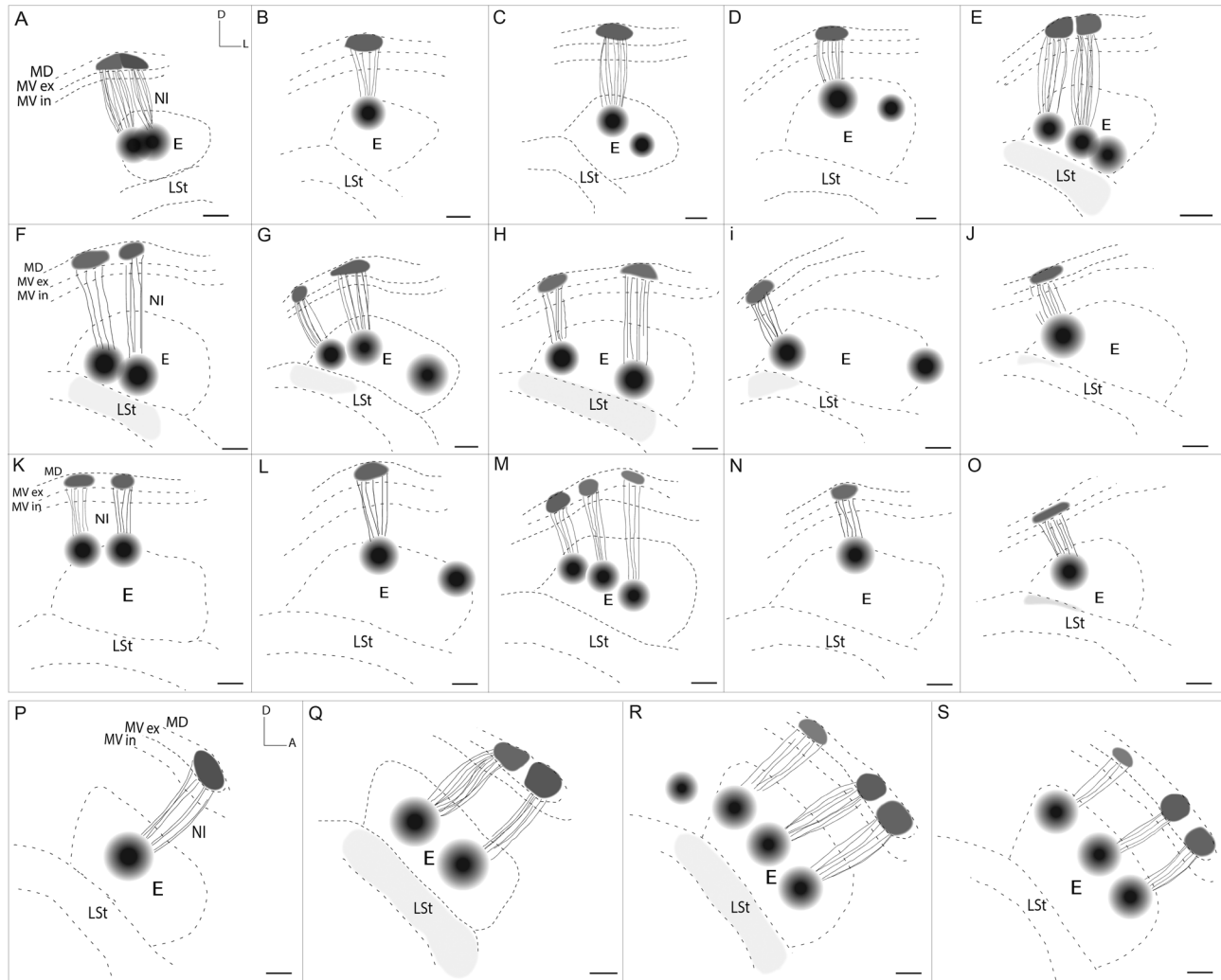
Figure 4. Double deposit of biocytin into the E in a transverse vital slice (500 µm thick) of the visual DVR. **A:** Histochemically reacted, Nissl-counterstained section (50 µm) taken from the experimental slice. Dashed lines indicated boundaries between the different zones. Asterisks indicated the position of the deposits. Note that the dorsal fields of labeled terminals are indeed located within the MVex. Note also a field of labeled terminals at the LSt. **B:** Detail of the lateral field of terminals at MVex. Incoming axons split into several fine branches, forming a dense mesh of terminals. Some individual axons (arrowheads) proceed farther. Scale bars = 200 µm.
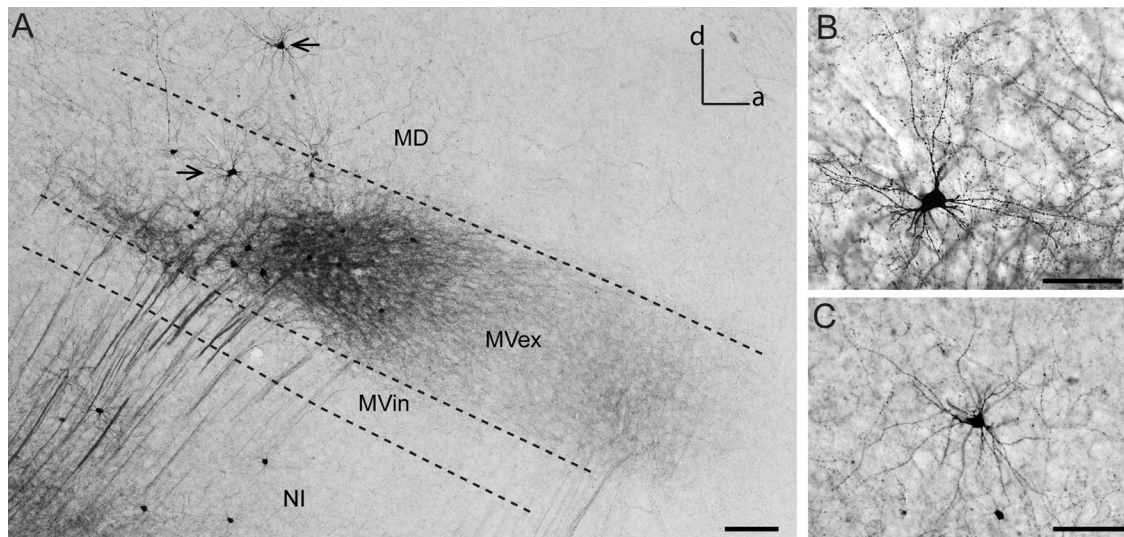
Figure 5. Retrogradely labeled cells and terminals at the MVex after a double deposit of biocytin into the E in a sagittal vital slice (500 µm thick) of the visual DVR. Photographs were taken from a histochemically reacted 50-µm section. **A:** Labeled terminals and cells at the MVex. Incoming axons form a dense mesh of very fine terminals. Several labeled cells appear intermingled within the terminal field. **B:** Retrogradely labeled cell at the MVex (arrow in A). **C:** Retrogradely labeled cell in MD (arrow in A). Note the characteristic spiny stellar morphology exhibited by these cells. Scale bars = 100 µm in A; 50 µm in B,C.

Deposits of crystals tracers into definite E loci revealed compact and discrete bundles of labeled fibers emerging from each of the injection sites (Figs. 2, 3, sagittal and coronal views, respectively). These fibers follow a straight, dorsoventral course across the NI and the MVint (Figs. 10B,C, 12A,C), finally to form a well-defined, dense terminal zone within a discrete locus at the MVex (Figs. 5, 10B,C). Confinement of the labeled terminals within the limits of the MVex was appreciable in unstained wet slices and was readily confirmed in the same slices after counterstaining with Nissl (Fig. 4). Individual terminals feature a dense mesh of varicose, fine processes that arise from the main axon at a single branching point. Furthermore, a characteristic cluster of retrogradely labeled cells of stellar morphology (see below) was evident in all cases (Figs. 5B,C, 10C,D). Most

Figure 6. Schematic representation of representative cases with single and multiple deposits of biocytin into the E. Each schema is a scaled-down version of a detailed camera lucida reconstruction of a histochemically reacted section taken from the experimental slice. Dashed lines indicate the boundaries between the different regions. Solid black represents crystal deposits. Dark gray represents terminal fields at the MV. Light gray represents terminal fields at the LSt. **A-O:** Rostral to caudal series of coronal slices. **P-S:** Sagittal slices. Labels in the left schema of each row apply to all schemas in the row. Note that the system of axonal columns span trough all rostrocaudal and lateromedial entopallial levels. Note also that the terminal fields at the LSt appear only in the cases in which the tracer deposits compromise the ventral aspect of the E. In some instances, crystal deposits do not result in transport of the tracer. Scale bars = 200 μm.

of these cells lie intermingled with the terminal fields, but some of them were located in the MD, restricted to the zone immediately adjacent to the terminal field (Figs. 3B, 5C). Rare retrogradely labeled cells and some labeled terminals were also found in the MVint, always in close contiguity with the MVex terminal fields.

When multiple deposits were made in the same slice (30 instances), the absence of processes running horizontally between the injection sites or between the resulting terminal fields was noteworthy. This is a strong indication of a columnar (between layers) rather than a horizontal (within layers) organization of these projections. We performed these multiple injections on

sagittal (15 instances) as well as transverse (15 instances) slices, sampling nearly all rostrocaudal and lateromedial aspects of E (Fig. 6). In all instances, we found that the position of the resulting labeled zones in the MVex covaried directly with the position of the injection sites in the E, indicating that this system of projections follows a precise, direct topographic arrangement. We found that this system of projections involves also the medial margin of the E and a corresponding portion of the medial aspect of the MVex (Fig. 7). This latter feature has not been described previously.

The results described above clearly indicate the existence of reciprocal, homotopic columnar projections
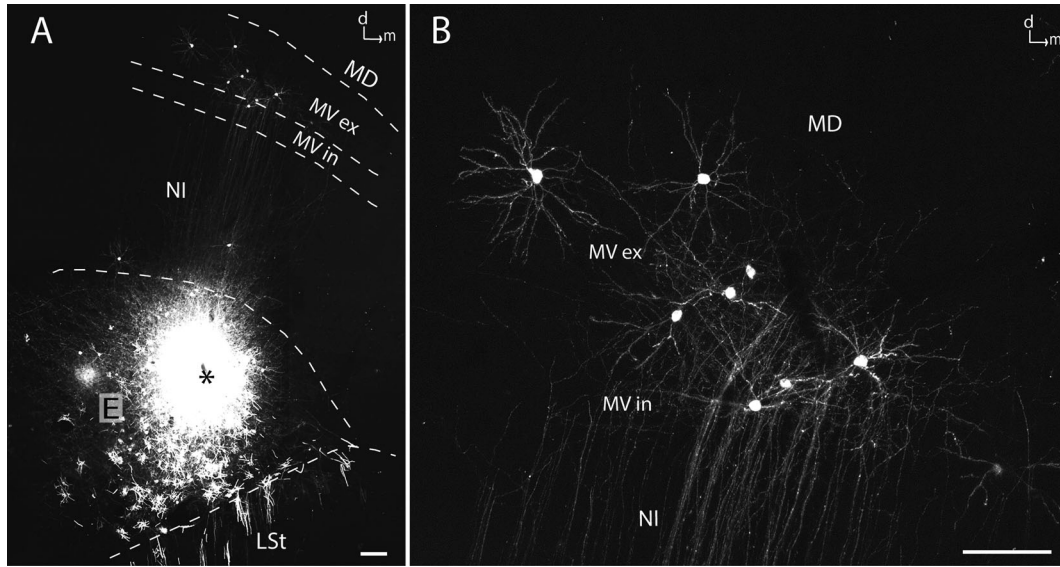
Figure 7. Single deposit of DiI into the medial margin of the E in a transverse vital slice (500 μm) of the visual DVR. Confocal images were obtained from a 50-μm section. Dashed lines indicated boundaries between the different regions. **A:** Crystal deposit and resulting pattern of label. Note that the labeled axons run toward a medially located locus at the MVex. **B:** Detail of the resulting retrogradely labeled cells at the MVex. Scale bars = 200 μm.
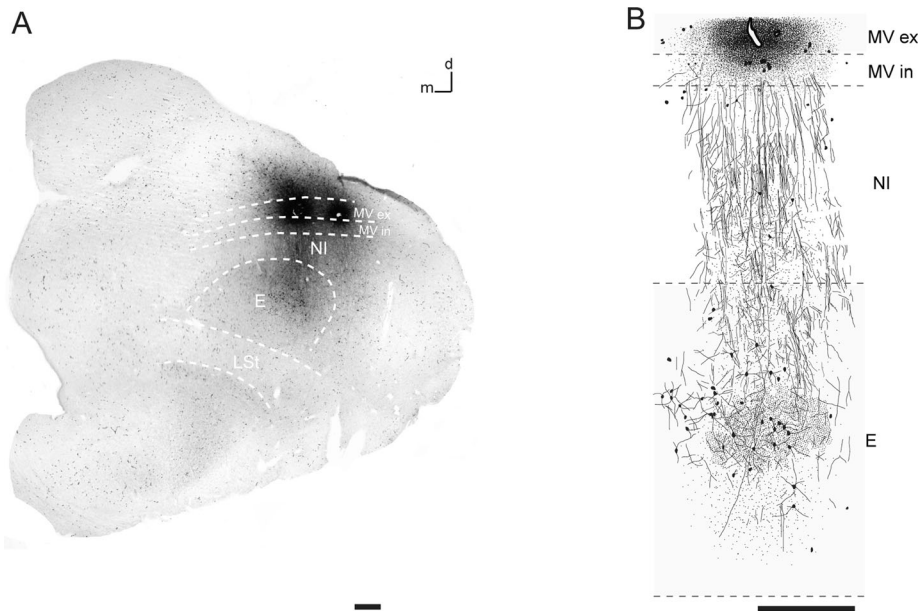

Figure 8. Double deposit of biocytin into the MVex in a transverse vital slice (500 μm thick) of the visual DVR. **A:** Histochemically reacted 50-μm section showing the deposit sites. Dashed lines indicated boundaries of the different regions. **B:** Camera lucida reconstruction of the "column" consequent to the medial deposit indicated in A. Compact black dots represent crystal deposit. Solid lines represent axonal processes. Fine dots represent axonal terminals. Note that retrogradely labeled cells appear mostly restricted to the dorsal aspect of the E. Labeled terminals are evident at the NI as well as at the Ed. Scale bars = 200 μm.

between the E and the MVex. Because the tracer deposits masked the putative "column-forming" elements at the entopallial side, we performed restricted injections of crystalline tracers into different loci of the MVex to characterize these hidden elements better (Figs. 8, 9, 10A,B). As expected, each of these injections resulted in the labeling of well-defined bundles of axons originating from the injection site and running in
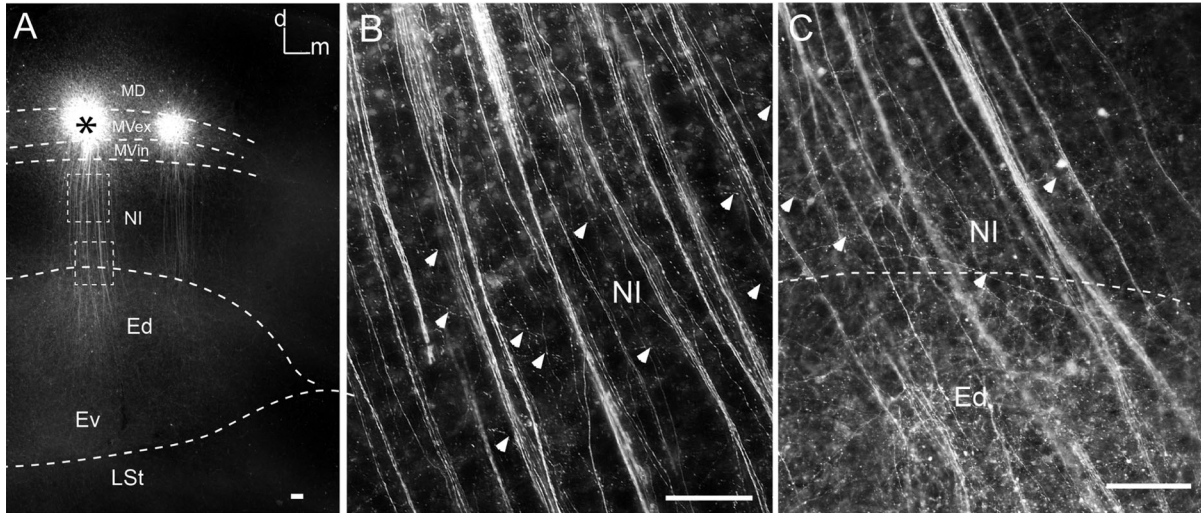
Figure 9. Multiple deposits of biocytin into the MVex in a coronal vital slice (500 μm thick) of the visual DVR. Photographs were taken from a histochemically reacted 50-μm section. Contrast was inverted for better visualization. **A:** Deposit sites. Dashed lines indicated boundaries of the different regions. Note the bundles of axons arising from each deposit and the corresponding terminal fields in the E. **B,C:** Details of the central "column" (asterisk in A). B: Detail of the superior boxed area. Note at the NI the fine axonal terminals arising from the main course of the axons (arrowheads). C: Detail of the inferior dashed area in A. Axonal terminals are evident at the NI as well as at the Ed. Scale bars = 200 μm.
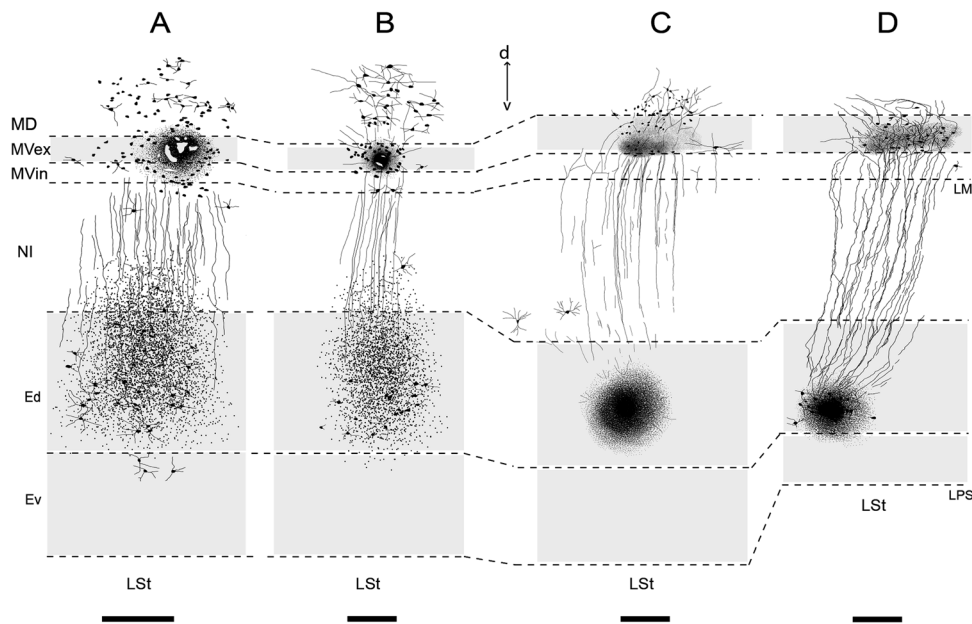
Figure 10. Camera lucida reconstructions of four representative cases of crystal deposits of biocytin into different components of the visual DVR. These were single deposits, performed each in a different transverse slice. Solid black represents crystal deposits. Solid lines represent axonal processes. Fine dots represent axonal terminals. Dashed lines indicated boundaries between the different regions. **A,B:** Deposits into the MVex. **C,D:** Deposits into the E. Labeled terminals at the NI were evident in A and B only. Note that retrogradely labeled cells at the E are restricted to its dorsalmost aspect in both A and B. Some retrogradely labeled cells are evident at the NI in different instances. See text for details. Ed, dorsal aspect of the entopallium; Ev: ventral aspect of the entopallium. Scale bars = 200 μm.

a straight course across the MVint and the NI, finally to terminate forming restricted terminal zones in the E (Figs. 8, 9). Labeled terminals in these zones were of low density and spanned the dorsal two-thirds of the E. However, occasionally we saw labeled axons running farther ventrally, reaching the pallial/subpallial border
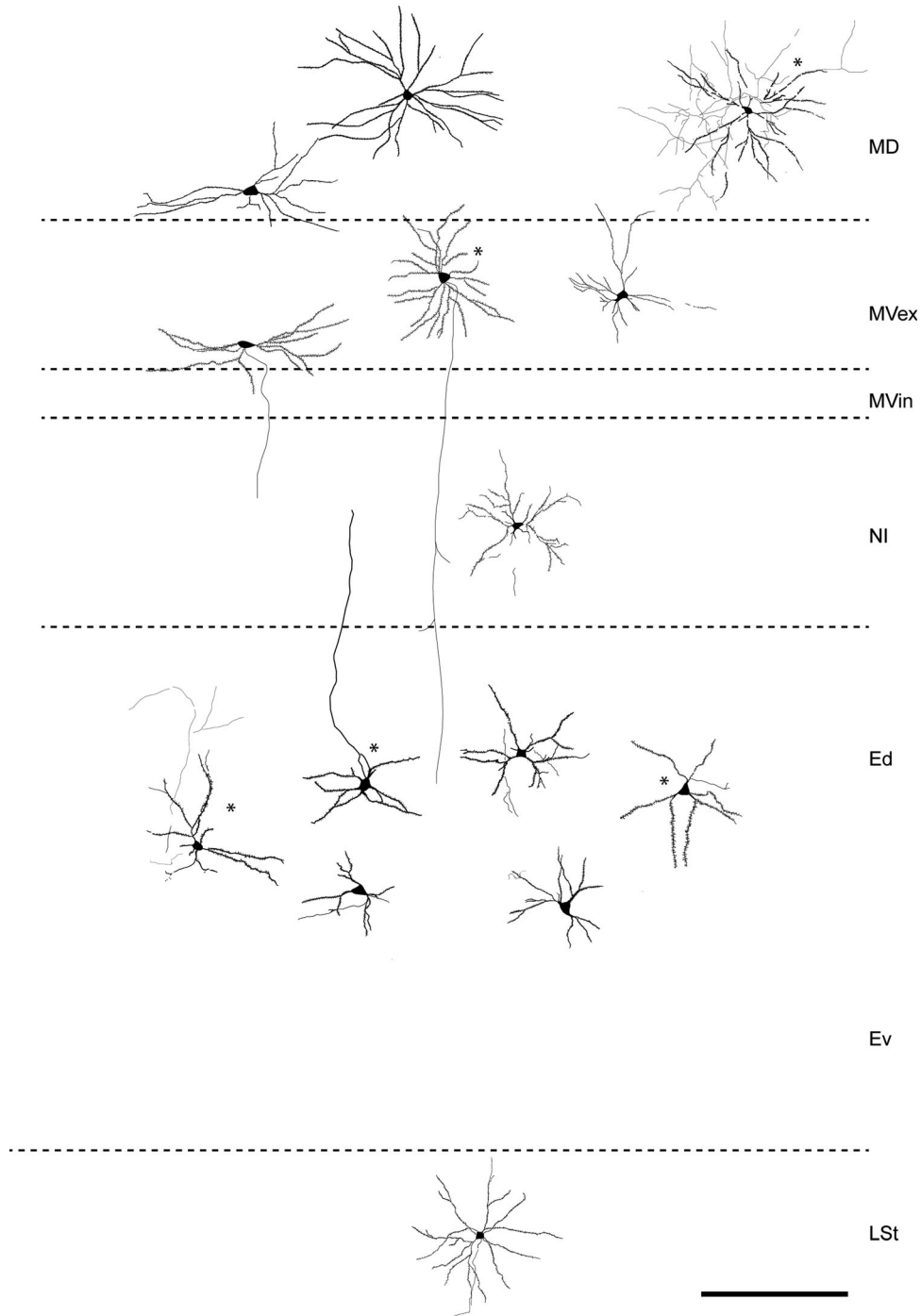
Figure 11. Cell types in the visual DVR. Camera lucida reconstructions. Laminar location of the cells is indicted. Asterisks indicate cell fillings. Scale bar = 200 μm.

(Figs. 8B, 10A,B). Individual terminals had a characteristic morphology, featuring short ramifications endowed with varicosities, which arose at regular intervals from the main axons (Figs. 9, 12B). Furthermore, a characteristic set of retrogradely labeled spiny stellate neurons (see below), located within and around the terminal zone, was evident in each of these instances.

In all cases, most of the labeled cells appeared to be distributed within the dorsal two-thirds of the E, including some located at the limit between the E and the NI (Fig. 10A,B). Retrogradely labeled cells located ventrally in the E were rare and appeared only in instances in which the injection site encompassed a portion of the MVint.
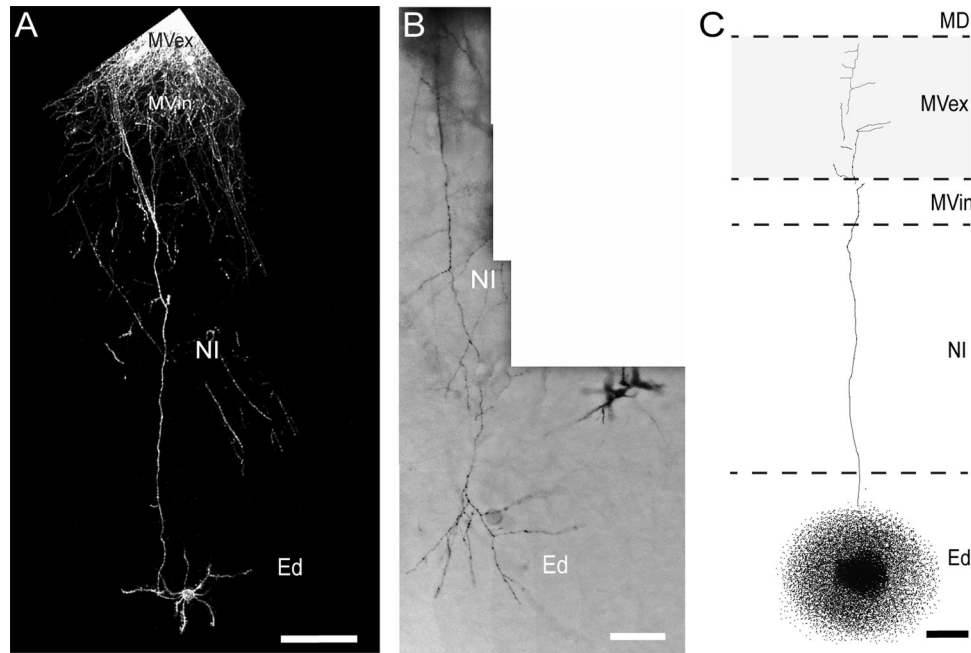
Figure 12. Representative "column-forming" elements. **A:** Confocal image of a entopallial cell retrogradely labeled from a DiI deposit in the MVex. The axon of this cell reaches the deposit site without giving rise to noticeable side branches at the NI. **B:** Confocal image of an axon anterogradely labeled after a deposit of DiI at the MVex (not shown). Note at the NI level several short branches departing from the main course. At the dorsal entopallium, the axon terminates, forming several varicose branches. **C:** Camera lucida reconstruction of an axon anterogradely labeled after a biocytin deposit into the dorsal entopallium. Note the fine terminal processes at the MVex/Md level. Scale bars = 50 μm in A,B; 100 μm in C.

## Column-forming cell types and projections

In several of the tracer experiments, a "Golgi like" quality of staining of retrogradely labeded cells was observed, as shown in Figures 5 and 7. This allowed us to study with some detail the morphology and projection pattern of the principal neuronal types involved in the columnar projections. Entopallial "column-forming" neurons had small to medium-sized polygonal cell bodies (major axis 15.5 ± 2.7 μm, mean area of 170 μm^2, n = 50) and featured a characteristic stellar morphology with multiple (five to seven), short primary dendrites departing radially from the soma. These dendrites exhibited abundant dendritic spines and gave rise to only one or two secondary branches (Fig. 11). Mesopallial column-forming neurons also had a stellate morphology, but they were larger than the entopallial cells (major axis 19.8 ± 2.4 μm, mean area 244 μm^2, n = 35) and featured more, longer, and more branched spiny primary dendrites. Camera lucida reconstructions of several of these cellular elements, some of them labeled by means of cell filling, are depicted in Figure 11.

Additionally, in several instances, it was possible to follow the entire course of individual axons from the injection sites to their corresponding terminal zones (Fig. 12). We found that most of the axons that we observed

departing from the E to the MVex did not give rise to noticeable side branches or collaterals at the NI level. In contrast, most of the axons from the MV to the E gave rise to several short branches that ended in fine varicosities as they ran through the NI, which suggests that the MV is a much more significant source of afferents to the NI than the E. These results indicate also that entopallial and mesopallial cells involved in interlaminar connections do not originate significant projections within their lamina of origin, further stressing the columnar organization of the interlaminar projections.

The ventral region of the entopallium gives rise to striatal projections

Deposit of either biocytin or DiI in E revealed the presence of axonal projections arising from the injected locus and following a ventral course toward the underlying lateral striatum. These axons were not of rotundal origin because they formed clear terminal fields within the LSt (Figs. 4A, 13). These E-LSt projections were evident only in cases in which the injection sites compromised the ventral aspect of the E (Figs. 6, 13). Injection sites contained within the dorsal oinethird of E did not give rise to striatal projections in any instances.
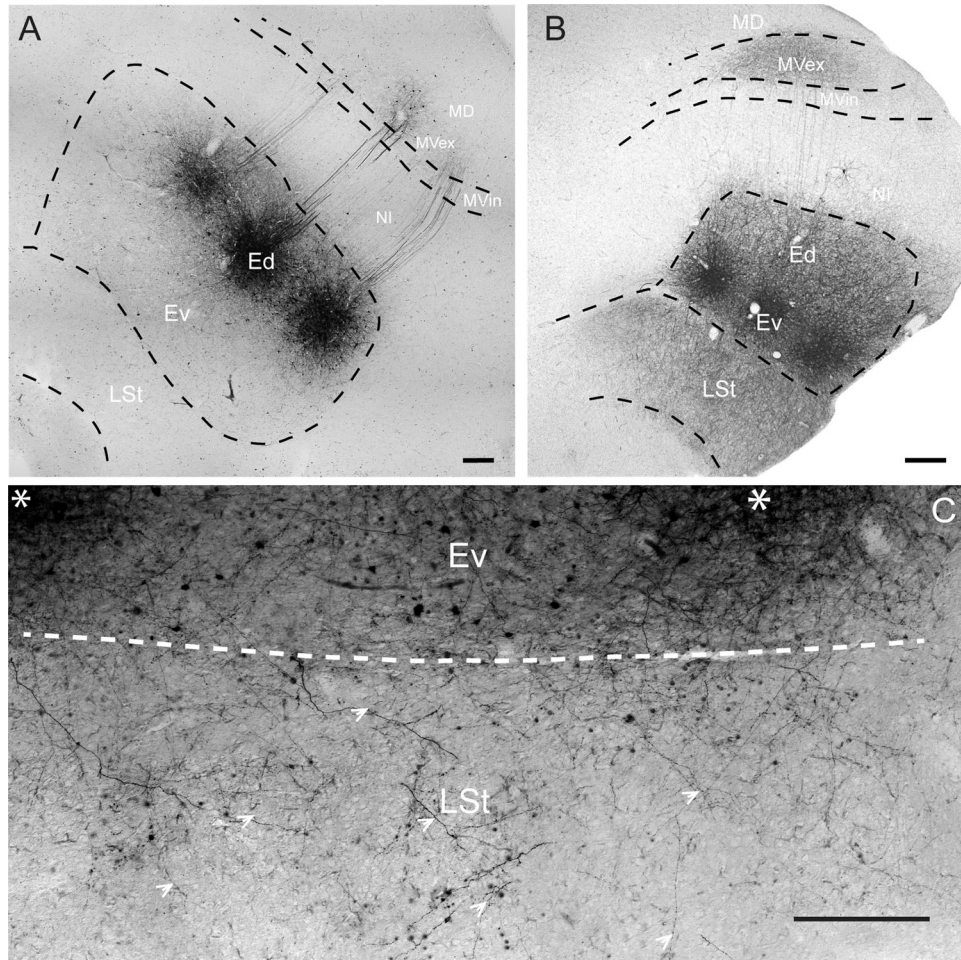
Figure 13. E-LSt projections. **A:** Microphotograph of a histochemically reacted section (50-µm) taken from a sagittal slice with multiple deposits of biocytin into the dorsal aspect of the E. Note that the LSt appears free of significant label. **B:** Histochemically reacted section taken from a "quasisagittal" slice with multiple deposits of biocytin into the ventral aspect of the E. The LSt appears outlined by a mesh of labeled processes. **C:** Microphotograph of a histochemically reacted section taken from a sagittal slice with two deposits of biocytin (asterisk) into the ventral E. In this case, the relative minor density of the resulting labeling at the LSt allows a clear visualization of individual labeled terminals (arrowheads). Scale bars = 200 µm in A,B; 100 µm in C.

DISCUSSION

Recent comparative studies have substantially stressed the similarities between mammalian and sauropsid's pallial territories. In particular, the pallial nature of the avian DVR, once controversial, has now been widely recognized. In addition, the homological correspondence between cell types that form specific nuclear masses of the DVR and cells types that form specific layers of the mammalian cortex (the nucleus-to-lamina hypothesis), proposed initially by Karten (1969), has gained considerable support, especially after several recent studies analyzing the expression of molecular markers (Jarvis et al., 2005, 2013; Butler et al., 2011; Dugas-Ford, 2012). However, possible similarities at the level of the interconnections and local circuits between pallial components have been emphasized less, mainly because of the relative scarcity of studies addressing in detail the internal organization of the sauropsid DVR. In this regard, the work of Wang et al. (2010) represents a substantial contribution because it shows the existence of recurrent local circuits within the components of the auditory DVR that closely resemble the columnar arrangement of the interlaminar circuits of the mammalian cortex.

Here we have explored the intrinsic organization of the avian visual DVR, with the aim of unraveling the specific pattern of connections among its different cellular components. As stated in the introductory paragraphs, the efferent connections of the E have been studied previously by several authors (Husband and Shimizu, 1999; Alpár and Tömböl, 2000; Laverghetta and Shimizu, 2003; Krützfeldt and Wild, 2004, 2005). These

studies have shown that the E provides short-range projections to three main targets, the underlying striatum, the "entopallial belt" or perientopallium (which we call NI), and the overlying MVL. However, a detailed analysis of these projections is still lacking. Our results confirm and extend these previous findings by showing that the cytoarchitecture and internal circuitry of the visual DVR are much more complex than previously appreciated and follow a pattern strikingly similar to that of the auditory DVR.

Visual DVR internal organization

We found that the entopallial-mesopallial projection described previously by Alpár and Tömböl (2000) and Krützfeldt and Wild (2005) is organized as a system of reciprocal projections formed by dorsoventrally oriented, discrete columnar bundles of axons, which follow a precise topographic homotopic arrangement between the two regions. Entopallial column-forming neurons were located mainly in the dorsal half of the E and featured a stellate morphology with a restricted number of relatively short, spiny, primary dendrites, which extended in all directions from the soma. The axonal terminals of these cells in the MV formed a dense band that clearly defined a laminar partition, which we call the MVex. These entopallial axons rarely extended collaterals to the NI, although we cannot discard the possibility that these axons established "en passant" synapses within the NI. In turn, MVex cells contributing to the columns were medium-sized neurons, also featuring spiny stellate morphology. Most of these cells were intermingled with the entopallial terminals at the MVex, but some of them were located dorsally, at the immediately adjacent MD. Axons of these cells en route to the E frequently give rise to several branches toward the NI ending in several short ramifications across the dorsal two-thirds of the E, in close contact with the entopallial column-forming cells (see Fig. 12).

It is worthwhile to note a significant discrepancy between our results and those previously reported by Krützfeldt and Wild (2004, 2005). According to these authors, E-MV projections originate from cells located in ventral aspect of the E, whereas our results indicate that these cells are mostly restricted to the dorsal half of the E. This discrepancy might be due in part to the different methods employed. We performed minute injections of crystalline tracers into brain slices, a method that allows maximizing the precision of the location and extension of the tracer deposits, whereas Krützfeldt and Wild performed "in vivo" injections of tracer solutions, a method that is inherently more uncertain with regard to location and extension of the tracer placements. Such methodological differences may be important when dealing with small brain structures.

We were unable to find clear evidence showing the involvement of projections from cells of the NI or the MVint in the intrapalial circuits described above. Retrogradely labeled cells in the NI were evident only in those experiments in which the tracer injections were localized close to the MV/NI border and were very infrequent or absent in all other cases. This result hints at the existence of NI projections to the internal most lamina of the MV. We attempted to address this question by performing intracellular fillings of NI cells in brain slices. Our preliminary results show that NI is formed by large stellate cells, with multiple primary spiny dendrites. The axons of these cells split into several fine branches shortly after departing from the soma. Some of these branches appear to follow an ascending course toward the MV and others a descending course toward the entopallium. Unfortunately, so far, we have not been able to follow the entire course of these branches to their end targets. The detailed morphological characterization of the cell types forming the internal circuits of the visual DVR will require further studies.

Previous authors have described how projections from the visual DVR to other pallial zones, such as the arcopallium and the laterofrontal and laterocaudal nidopallium, arise mainly from cells in the NI and to a minor extent from cells in the E (Husband and Shimizu, 1999; Krützfeld and Wild, 2005). It has to be noted that in these previous studies the NI appear to be designated partially or totally as "perientopallium" (Ep/Ep2). We have recently started a reevaluation of this question, performing restricted retrogradely tracer injections into the pallial targets of the visual DVR (Fernández et al., 2013). Our initial results indicate that projections from the visual DVR originate exclusively from cells in the NI, with no noticeable involvement of cells in the E or the MV. These projections appear to be topographically organized and seem to originate from different subpopulations of cells intermingled within the NI. Thus, instead of a uniform cell mass, the NI may be envisaged as being composed of different types of specialized neurons, involved in long-range intrapalial projections and perhaps also in short-range projections within the visual DVR.

On the other hand, several lines of evidence suggest that the NI may receive sparse projections from the Rt. After large injections of CTb into the Rt, anterograde labeled rotundal fibers appear to form a diffuse "crown" that arises from the E and extends across the internalmost aspect of the NI. That same crown of fibers is also very evident in wet, unstained tissue (see Figs. 1

and 2 of Fredes et al. 2010). Furthermore, we previously found that injections of DiI crystals into the NI of pigeons "in vivo" resulted in the labeling of substantial numbers of cells in the Rt (Ahumada et al., 2012). However, after more local injections of CTb into the Rt, only very few labeled fibers and terminals could be found at the NI (unpublished result). In most instances, these fibers enter the NI from the E, suggesting that they arise as collaterals of the Rt-E fibers. Thus, in addition to the entopallium, which receives very dense afferents from the Rt, the visual DVR may contain a more external thalamorecipient layer, the NI, receiving sparse afferents from Rt. In the absence of more definitive studies, it is difficult to assess the functional relevance of the Rt-NI projection, but its existence cannot be overlooked. In particular, the cells of origin of this projection as well its synaptic targets should be clarified further.

Given these results, the visual DVR can be understood as a complex composed of three main differentiated layers, internal (thalamorecipient, E), intermediate (efferent, NI), and external (associative, MV). Each of these layers appears to be composed of specific sublayers. Interconnections among these layers seem to form operational modules in which cells located in homotopic positions in each layer would be synaptically linked by an interlaminar local loop of recurrent axonal processes. According this view, the activity of each module could be driven by an incoming thalamic axon and would result in the modulation of the activity of the efferent cells, which would be akin to the mechanism observed in mammalian intracortical circuits (see below). A detailed physiological analysis of the synaptic interactions that take place in this intrapallial circuit will be necessary to validate these conjectures. A schematic representation of these findings is presented in Figure 14.

The striatal connection

Entopallial projection to the adjacent lateral striatum has been described previously (Dubbeldam and Visser, 1987; Alpár and Tömböl, 2000). Krützfeldt and Wild (2004, 2005) described this projection as "robust" and showed that it arises from cells located in the internal most aspect of the E. In our experiments, we found that fiber bundles reaching the LSt were evident only after tracer injections compromising the internal half of the E (see Fig. 13). We found that these projections also appear to have a topographic/columnar arrangement because the bundles of labeled fibers arising from the injection site seemed to be spatially restricted and followed a straight course through the entopallial/
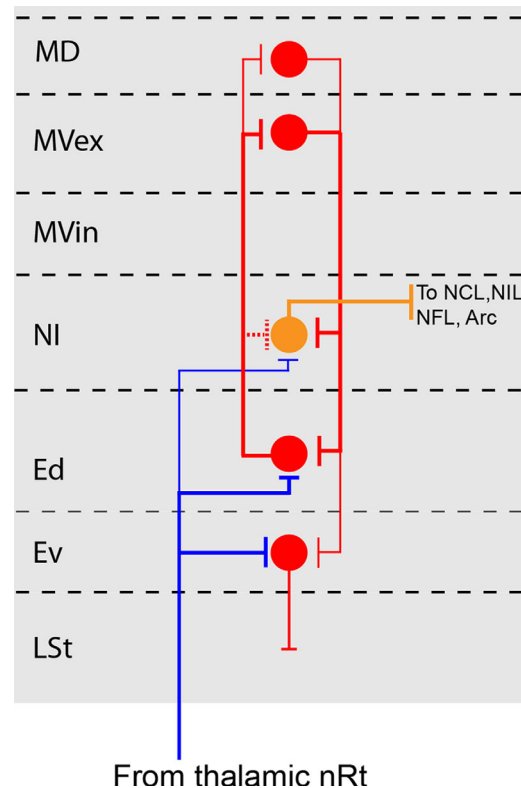
Figure 14. Visual DVR modular interlaminar circuit. The width of the lines represents the purported relative size of the indicated projections. Dashed lines indicate dubious but possible projections. See text for details. NCL, caudolateral nidopallium; NIL, intermediate-lateral nidopallium; NFL, frontolateral nidopallium; Arc, arcopallium. Other abbreviations as in Figure 1.

striatal junction, to end forming definite terminal domains within the LSt (Fig. 13).

Pallial projections to subpallial structures have been extensively documented in mammals. These projections arise from pyramidal cells located mostly at layer V in all cortical regions, including sensory areas (McGeorge and Faull, 1989). In contrast, projections from the thalamorecipient cortical layer IV to the striatum are not known to exist in primary sensory cortices. Thus, projections to the striatum from the thalamorecipient region of the visual DVR, such as the one demonstrated here, may represent a feature peculiar to the avian clade and seem to indicate that the influence of sensory processes on subpallial structures is more direct in birds than in mammals.

Subdivisions of the entopallium

The entopallium shows no obvious subdivisions on the basis of cytoarchitecture (Rehkamper et al., 1985) or cellular morphology (Tömböl et al., 1988; Tömböl, 1991). Parcelations of E based on the distribution of

several neurochemicals, such as parvalbumin and calbindin, have produced somewhat inconsistent results (Brauth et al., 1986; Dietl and Palacios, 1988; Veenman and Reiner, 1994; Veenman et al., 1994; Hellmann et al., 1995). Karten and Hodos (1970) first proposed a partition of the E into an internal "core" (Ec) and an external "belt" (Ep), based on cytoarchitectonic differences and differential density of rotundal afferents as assessed by axonal degeneration methods. As noted above, the term "Ep" was subsequently used in several studies to designate totally or partially the NI region, introducing some degree of confusion into the literature. Despite methodological differences and "semantic" discrepancies, the segregation proposed by Karten and Hodos coincides, albeit not exactly, with the partition of the E into an internal (ventral, Ei) and an external (dorsal, Ex) domain, proposed later by Krützfeldt and Wild (2004, 2005), based on cytoarchitecture, immunohistochemical properties, and differential density of rotundal endings as assessed by tract tracing methods. In this regard, our results lend further support to this segregation; we suggest, based on differential projections patterns, that the entopallium may be constituted by two different populations of neurons, an internal, LSt-projecting group and a more external, MV-projecting group.

On the other hand, several tract tracing experiments support the notion that separate portions of E receive afferent projections from the different subdivision of the Rt in a way that maintains the rostrocaudal order of the rotundal subdivisions (Benowitz and Karten, 1976; Nixdorf and Bishof, 1982; Laverghetta and Shimizu, 2003; Krützfeldt and Wild, 2005). In the most recent of these studies, Fredes et al. (2010) investigated in detail the topography of the Rt-E projections in the pigeon, identifying three rostrocaudally segregated entopallial regions, anterior, central, and posterior, each of which receives afferents from a specific Rt subdivision. In addition, Fredes et al. show that the projections from each of the Rt subdivisions to their corresponding entopallial targets followed a strict topographic order. Considering the shape and spatial arrangement of the entopallial areas, Fredes et al. (2010) proposed that the central area, which receives afferents from the central subdivision of Rt, corresponds to the internal entopallial domain (Ei) described by Krützfeldt and Wild (2004, 2005) and hinted at in the present study. The external domain (Ex) would then correspond as a whole to the anterior and posterior entopallial areas, which receive afferents mainly from the dorsal anterior and posterior subdivisions of Rt respectively.

This issue is of relevance because Rt subdivisions are known to receive projections from different populations of tectal ganglion cells and to exhibit different visual sensorial properties and appear to mediate the perception of different visual attributes (Benowitz and Karten, 1976; Wang et al., 1993; Mpodozis et al., 1996; Karten et al., 1997; Hellmann and Güntünkün, 2001; Marin et al., 2003). Thus, one can expect the existence of an anatomical and functional segregation within the E reflecting the segregation of visual channels that is apparent at the Rt. In fact, behavioral experiments show that bilateral lesions in the caudal or the rostral entopallium of trained pigeons results in differential discrimination deficits for motion or a grating task, respectively (Nguyen et al., 2004). At present, however, it is unclear how, and to which extent, this expected segregation takes places, both at the E and in its subsequent projections. By considering together our results and the proposition from Fredes et al. (2010), we speculate that one of the labeled lines forming the tectofugal system, specifically the one involving the central entopallium, is concerned mainly with interactions with subpallial structures, although the other two discernible labeled lines, those involving the rostral and caudal entopallium, contribute to the columnar system of interactions with other components of the visual pallium. Alternatively, one can also speculate that each of the entopallial subdivisions, and hence each of the labeled lines composing the tectofugal system, may give rise, at the entopallial level, to a dorsal, pallial (MV)-projecting stream and a ventral, subpallial (LSt)-projecting stream. Distinguishing between these two alternatives will require a careful anatomical study of the efference of each of the entopallial areas.

The columnar organization of the sensorial DVR

It is easy to appreciate the striking similarities between the organization of the visual DVR revealed here and the organization of the auditory DVR (Wang et al., 2010). In both cases, the most salient feature is the presence of a system of axonal columns connecting reciprocally a sensory recipient nidopallial territory with an overlaying mesopallial territory. In both cases an intermediate nidopallial territory, also receiving the columnar axons, originates projections toward other pallial areas. In addition, in both cases these major layers appear to contain specialized sublayers, distinguishable both cytoarchitectonically and by their specific connections within the local circuit. Furthermore, the main cells types forming these circuits exhibit similar morphology, even when the entopallial column-forming cells appear to be larger than their auditory counterparts.

Moreover, this columnar organization seems not to be restricted to the auditory and visual DVR but also appears to extend to the somatosensory DVR. In fact, even when the issue has not been addressed in detail, results reported from several studies suggest that the nidopallial nucleus basalis, which receives trigeminally derived somatosensory afferents, send topographic projections in turn toward the overlaying mesopallial zone (Dubbeldam and Visser, 1984; Atoji and Wild, 2012). We have obtained preliminary data indicating that this projection follows a highly organized columnar arrangement strikingly reminiscent of the one illustrated here (Ahumada, Fernandez, and Mpodozis, unpublished data). Our results also hint at the existence of projections from nucleus basalis to the adjacent striatal region, further suggesting strong similarities in the organization of the visual and somatosensory DVR territories.

In addition to sensory territories, the DVR contains several associative regions, which are also formed by the apposition of cytoarchitectonically distinct zones, such as the frontal and caudal divisions of the lateral pallium and the archopallium. A detailed study of the internal organization of these associative regions is necessary to clarify whether the "columnar principle" can be extended to the DVR as a whole.

Organization of the ammniote pallium: radial columns or recurrent local circuits?

From the initial works of Mountcastle and his colleges (1955, 1957), the concept of cortical column has become a fundamental framework for the study of sensorial and cognitive brain functions in mammals (Mountcastle, 1997). However, although physiologically defined columns have been characterized and extensively studied in a diversity of cortical areas, the "anatomical reality" of the cortical columns has remained elusive. In particular, it has been difficult to characterize, within the complex network of diverse cell types and synaptic interactions forming the cortex, anatomically defined modules matching the spatial dimensions of the physiological columns (Horton and Adams, 2005; for review see Da Costa and Martin, 2010).

The attempts to reconcile this apparent mismatch between the functional and the anatomical architecture of the cortex have led to the proposal of a "canonical cortical circuit" (Douglas and Martin, 1991). According to this proposition, the cortex should be envisaged as composed of repetitive local interlaminar circuits, whose operation gives rise to dynamically defined neuronal ensembles that act as basic computational modules. A fundamental feature of these canonical circuits is the existence of reciprocal, homotopical synaptic interactions between superficial and deep cortical layers. In the case of the sensory cortices, it is thought that these canonical circuits act on the incoming thalamic axons, amplifying and gating sensory-related activity toward other brain regions.

Overall, the accumulated evidence leads us to hypothesize that, despite the differences in cytoarchitecture and cell morphology (see Wild and Krützfeldt, 2010), the avian and mammalian pallium seem to embody a common operational organization that might be called a "canonical pallial circuit." Both structures appear to share at least a comparable pattern of internal connectivity, which includes as a relevant feature the presence of local interlaminar recurrent circuits driven by the thalamic afferents. Further support for this hypothesis will require additional, detailed, anatomical and physiological studies of the organization of the DVR. Preliminary physiological experiments from our laboratory have shown that electric stimulation of a discrete locus in the entopallium elicits a spatially restricted profile of activity across all layers of the visual DVR, which is consistent with a columnar organization in the DVR (Fernandez and Mpodozis, unpublished results; see also Engelage and Bischof, 1989). Such results indicate that the notion of a canonical pallial circuit has at least a heuristic value for the study of the visual DVR and thus deserves to be considered further.

CONCLUSIONS

Despite the phylogenetic distance between birds and mammals, avian and mammalian pallial territories appear to share a high degree of homological correspondence at the hodological, cellular, embryological, and developmental genetic levels (Aboitiz, 2011; Dugas-Ford et al., 2012; Jarvis et al., 2013). In addition, and according to our results, these structures may also share a common operational principle, which we have called the "canonical pallial circuit."

Anatomical differences between these structures, however, cannot be overlooked because they reflect the different evolutionary trajectories that these lineages have followed upon divergence from their common ancestor. In particular, the cytoarchitectonic layout, as well as the morphological features of some of its constituent cellular types, appears characteristically different in each case. Pyramidal cells, perhaps the more conspicuous cell type of the mammalian cortex, seem to be absent in the avian pallium.

As a result of these differences, the hypothesized canonical pallial circuits of birds and mammals would have to be implemented by different structural substrates. For example, whereas in birds only axonal processes participate in interlaminar interactions, in

mammals both axonal processes and specialized dendrites of the pyramidal cells participate of these interactions. Under these circumstances, the question of whether this hypothesized common operational organization stems from common ancestry or is the result of an evolutionary convergence becomes highly interesting. A common ancestry would imply that an operational feature, i.e., a network of synaptic relationships between neuronal elements, can be conserved during evolution independently of the conservation of the actual elements performing such operation. Extensive comparative studies, including other groups of amniotes, will be needed to answer these questions.

ACKNOWLEDGMENTS

CONFLICT OF INTEREST STATEMENT

The authors declare that they have no conflicts of interest.

ROLE OF AUTHORS

All authors had full access to all data in the study and take responsibility for the integrity of the data and the accuracy of data analysis. Study concept and design: PA-G, JCL, GJM, JM. Acquisition of data: PA-G, MF. Analysis and interpretation of data: PA-G, MF, GJM, JCL, JM. Drafting of the manuscript: PA-G, JM. Critical revision of the manuscript: PA-G, MF, JCL, GJM, JM. Obtained funding: JM, JCL. Study supervision: JM.

LITERATURE CITED

Aboitiz F. 2011. Genetic and developmental homology in amniote brains. Toward conciliating radical views of brain evolution. Brain Res Bull 84:125–136.

Ahumada P, Tapia S, Fernández M, Letelier JC, Marin G, Mpodozis J. 2012. Modular recurrent circuits in the avian visual collopallium. Program 895.04, Neuroscience Meeting Planner, New Orleans, LA, Society for Neuroscience Online.

Alpár A, Tömböl T. 2000. Efferent connections of the ectostriatal core.An Efferent connections of the ectostriatal core. An ananterograde tracer study. Anat Anz 182:101–110.

Atoji Y, Wild JM. 2012. Afferent and efferent projections of the mesopallium in the pigeon (Columba livia). J Comp Neurol 520:717–741.

Benowitz LI, Karten HJ. 1976. Organization of the tectofugal pathway in the pigeon: a retrogradely transport study. J Comp Neurol 167:503–520.

Brauth SE, Kitt CA, Reiner A, Quirion R. 1986. Neurotensin binding sites in the forebrain and midbrain of the pigeon. J Comp Neurol 253:358–373.

Butler AB, Hodos W. 2005. Comparative vertebrate neuroanatomy. Evolution and adaptation, 2nd Edn. John Wiley and sons.

Butler AB, Reiner A, Karten HJ. 2011. Evolution of the amniote pallium and the origins of mammalian neocortex. Ann N Y Acad Sci 1225:14–27.

Da Costa NM, Martin AC. 2010. Whose cortical column would that be? Front Neuroanat 4:1–10.

Dietl MM, Palacios JM. 1988. Neurotransmitter receptors in the avian brain. I. Dopamine receptors. Brain Res 439:354–359.

Douglas RJ, Martin KA. 1991. A functional microcircuit for cat visual cortex. J Physiol 440:735–769.

Dubbeldam JL, Visser AM. 1984. The organization of the nucleus basalis—neostriatum complex of the mallard (Anas platyrhynchos L) and its connections with the archistriatum and the paleostriatum complex. Neuroscience 21:487–517.

Dugas-Ford J, Rowell JJ, Ragsdale CW. 2012. Cell-type homologies and the origins of the neocortex. Proc Natl Acad Sci U S A 109:16974–16979.

Engelage J, Bischof HJ. 1989. Flash evoked potentials in the ectostriatum of the zebra finch: a current source-density analysis. Exp Brain Res 74:563–572.

Fernández M, Ahumada P, Sentis E, Letelier JC, Marin G, Mpodozis J. 2013. Intrapallial projections of the avian visual entopallial/mesopallial complex. A study in the pigeon. Program 64.07, Neuroscience Meeting Planner, San Diego, CA, Society for Neuroscience.

Fredes F, Tapia S, Letelier JC, Marín G, Mpodozis J. 2010. Topographic arrangement of the rotundo-entopallial projection in the pigeon (Columba livia). J Comp Neurol 518: 4342–4361.

Gilbert C, Wiesel T. 1989. Columnar specificity of intrinsic horizontal and corticocortical connections in cat visual cortex. J Neurosci 9:2432–2442.

Güntürkün O, Kröner S. 1999. A polysensory pathway to the forebrain of the pigeon: the ascending projections of the nucleus dorsolateralis posterior thalami (DLP). Eur J Morphol 37:185–189.

Hellmann B, Güntürkün O. 2001. Structural organization of parallel information processing within the tectofugal visual system of the pigeon. J Comp Neurol 429:94–112.

Hellmann B, Waldmann C, Güntürkün O. 1995. Cytochrome oxidase activity reveals parcellations of the pigeon's ectostriatum. Neuroreport 6:881–885.

Horton JC, Adams DL. 2005. The cortical column: a structure without a function. Philos Trans R Soc Lond B Biol Sci 360:837–862.

Husband SA, Shimizu T. 1999. Efferent projections of the ectostriatum in the pigeon (Columba livia). J Comp Neurol 406:329–345.

Jarvis ED, Güntürkün O, Bruce L, Csillag A, Karten H, Kuenzel W, Medina L, Paxinos G, Perkel DJ, Shimizu T, Striedter G, Wild JM, Ball GF, Dugas-Ford J, Durand SE, Hough GE, Husband S, Kubikova L, Lee DW, Mello CV, Powers A, Siang C, Smulders TV, Wada K, White SA, Yamamoto K, Yu J, Reiner A, Butler AB. 2005. Avian brains and a new understanding of vertebrate brain evolution. Nat Rev Neurosci 6:151–159.

Jarvis ED, Yu J, Rivas MV, Horita H, Feenders G, Whitney O, Jarvis SC, Jarvis ER, Kubikova L, Puck AE, Siang-Bakshi C, Martin S, McElroy M, Hara E, Howard J, Pfenning A, Mouritsen H, Chen CC, Wada K. 2013. Global view of the functional molecular organization of the avian

cerebrum: mirror images and functional columns. J Comp Neurol 521:3614–3665.

Karten HJ. 1969. The organization of the avian telencephalon and some speculations on the phylogeny of the amniote telencephalon. Ann N Y Acad Sci 167:164–179.

Karten HJ, Hodos W. 1967. A stereotaxic atlas of pigeon brain (*Columba livia*). Baltimore: The Johns Hopkins Press.

Karten HJ, Hodos W. 1970. Telencephalic projections of the nucleus rotundus in the pigeon (*Columba livia*). J Comp Neurol 140:35–51.

Karten HJ, Cox K, Mpodozis J. 1997. Two distinct populations of tectal neurons have unique connections within the tectorotundal pathway of the pigeon (*Columba livia*). J Comp Neurol 387:449–465.

Korzeniewska E, Gunturkun O. 1990. Sensory properties and afferents of the N. dorsolateralis porterior thalami of the pigeon. J Comp Neurol 292:457–479.

Krützfeldt NO, Wild JM. 2004. Definition and connections of the entopallium in the zebra finch (*Taeniopygia guttata*). J Comp Neurol 468:452–465.

Krützfeldt NO, Wild JM. 2005. Definition and novel connections of the entopallium in the pigeon (*Columba livia*). J Comp Neurol 490:40–56.

Laverghetta AV, Shimizu T. 2003. Organization of the ectostriatum based on afferent connections in the zebra finch (*Taeniopygia guttata*). Brain Res 963:101–112.

Marin G, Letelier JC, Henny P, Sentis E, Farfan G, Fredes T, Pohl N, Karten HJ, Mpodozis J. 2003. Spatial organization of the pigeon tectorotundal pathway: an interdigitating topographic arrangement. J Comp Neurol 458:361–380.

McGeorge AJ, Faull RL. 1989. The organization of the projection from the cerebral cortex to the striatum in the rat. Neuroscience 29:503–537.

Mpodozis J, Cox K, Shimizu T, Bischof HJ, Woodson W, Karten HJ. 1996. GABAergic inputs to the nucleus rotundus (pulvinar inferior) of the pigeon (*Columba livia*). J Comp Neurol 374:204–222.

Mountcastle VB. 1957. Modality and topographic properties of single neurons of cat's somatic sensory cortex. J Neurophysiol 20:408–434.

Mountcastle VB. 1997. The columnar organization of the neocortex. Brain 120:701–722.

Mountcastle VB, Berman AL, Davies PW. 1955. Topographic organization and modality representation in first somatic area of cat's cerebral cortex by method of single unit analysis. Am J Physiol 183:646.

Murakami Y, Uchidab K, Rijlia FM, Kuratani S. 2005. Evolution of the brain developmental plan: insights from agnathans. Dev Biol 280:249–259.

Nguyen AP, Spetch ML, Crowder NA, Winship IR, Hurd PL, Wylie DR. 2004. A dissociation of spatial-pattern vision in the avian telencephalon: implications for the evolution of "visual streams." J Neurosci 24:4962–4970.

Rehkamper G, Zilles K, Schleicher A. 1985. A quantitative approach to cytoarchitectonics. X. The areal pattern of the neostriatum in the domestic pigeon, *Columba livia* f.d. A cyto- and myeloarchitectonical study. Anat Embryol (Berl) 171:345–355.

Reiner A, Perkel DJ, Bruce LL, Butler AB, Csillag A, Kuenzel W, Medina L, Paxinos G, Shimizu T, Striedter G, Wild M; Ball GF, Durand S, Günturkün O, Lee DW, Mello CV, Powers A, White AS, Hough G, Kubikova L, Smulders TV, Wada K, Dugas-Ford J, Husband S, Yamamoto K, Yu J, Siang C, Jarvis ED. 2004. Revised nomenclature for avian telencephalon and some related brainstem nuclei. J Comp Neurol 473:377–414.

Sol D, Garcia N, Iwaniuk A, Davis K, Meade A, Boyle WA, Szekely T. 2010. Evolutionary divergence in brain size between migratory and resident birds. PLoS One 5:1–8.Find all citations in this journal (defaulOr filter your current search .

Striedter GF. 1997. The telencephalon of tetrapods in evolution. Brain Behav Evol 49:179–213.

Tömböl T. 1991. Arborization of afferent fibers in ectostriatum centrale. Golgi study. J Hirnforsch 32:563–575.

Tömböl T, Maglóczky Z, Stewart MG, Csillag A. 1988. The structure of chicken ectostriatum. I. Golgi study. J Hirnforsch 29:525–546.

Veenman CL, Reiner A. 1994. The distribution of GABA-containing perikarya, fibers, and terminals in the forebrain and midbrain of pigeons, with particular reference to the basal ganglia and its projection targets. J Comp Neurol 339:209–250.

Veenman CL, Albin RL, Richfield EC, Reiner A. 1994. Distributions of $GABA_A$, $GABA_B$, and benzodiazepine receptors in the forebrain and midbrain of pigeons. J Comp Neurol 344:161–189.

Wang YC, Jiang S, Frost B. 1993. Visual processing in pigeon nucleus rotundus: luminance, color, motion and looming subdivisions. Vis Neurosci 10:21–30.

Wang Y, Luksch H, Brecha N, Karten HJ. 2006. Columnar projections from the cholinergic nucleus isthmi to the optic tectum in chicks (*Gallus gallus*): a possible substrate for synchronizing tectal channels. J Comp Neurol 494:7–35.

Wang Y, Brzozowska-Prechtl A, Karten HJ. 2010. Laminar and columnar auditory cortex in avian brain. Proc Natl Acad Sci U S A 107:12676–12681.

Wild JM, Krützfeldt NO. 2010. Neocortical-like organization of avian auditory cortex. Commentary on Wang Y, Brzozowska-Prechtl A, Karten HJ (2010): Laminar and columnar auditory cortex in avian brain. Proc Natl Acad Sci U S A 107:12676–12681. Brain Behav Evol 76:89–92.